

Short Research Article

1 Numerical analysis of an unsaturated capillary barrier cover system

6 Abstract

7 Waste management of landfills is a vital challenge for developing countries. In a landfill facility contaminant are
8 unintentionally removed from a waste pile through water infiltration, which consequently leads to soil and
9 groundwater pollution. To protect landfill facilities and diminish the risk of contaminant migration to soil and
10 groundwater, inclined multi-layered barriers can be used to confine the infiltration through implementation of the
11 capillary barrier effect. In this study, the effect of rainfall, evaporation, and transpiration on the hydraulic properties
12 of inclined covers was assessed by performing a series of simulations using HYDRUS-2D numerical models. Key
13 results were used to evaluate the response of multi-layered inclined capillary cover barriers. The material of the
14 intended layers included clay loam soil as a seepage control layer, sandy soil as a moisture retention layer, and gravel
15 as a capillary break layer. Based on the key results of numerical analyses, Darcian velocity in the moisture retention
16 layer was nearly constant throughout the slope due to the hydraulic properties of the materials and the pressure
17 head. Lateral diversion in the interface between the seepage control layer and moisture retention layer occurred as
18 a result of the significant slope of said layers and the low permeability of the moisture retention layer. At the reduced
19 degree of saturation, water did not move easily from the seepage control layer to the moisture retention layer as
20 well as from the moisture retention layer to the capillary break layer due to the low hydraulic conductivity. The
21 negative pressure head in the seepage control layer – caused by evapotranspiration, surface runoff, and lateral
22 drainage – had minimal effect on the water content in the moisture retention layer. Water content increased in the
23 seepage control layer and the moisture retention layer during the first 10-year period simulation, which
24 demonstrated a reliable prediction.

25 Keywords: Capillary Cover Barriers; Retention Capacity; Hydraulic Properties; Suction; Volumetric Water Content

26 **1. Introduction**

27 In humid regions, waste can be considered a serious threat to ground water due to percolation from infrastructures
28 such as landfills, which are the current preferred solution for disposal. (*Khire, M.V., Benson, C.H., and Bosscher, P.J.*
29 *2000*).

30 The percolation into underlying waste in these regions can be reduced through covers made up of earthen materials
31 for promotion of the capillary barrier effect (*Zaradny 1993, Morris and Stormont 1997, Bussière, Aubertin, Chapuis.*
32 *2003, Mallants, Volckaert, Marivoet. 1999, Aubertin, M. Cifuentes, E. Apithy, S.A. Bussière, B. Molson, J, Chapuis, R.P.*
33 *2009*). Earthen covers are designed in various forms but are comprised of multi-layered contrasting particle sizes
34 that consist of fine-grained and coarse-grained sediments (*Zaslavsky and Sinai 1981a, b; Nieber and Walter 1981;*
35 *Stagnitti, F., Parlange, J.-Y., Steenhuis, T.S., Parlange, M.B., and Rose, C.W. 1992; Selim 1988; Steenhuis, T.S.,*
36 *Parlange, J.-Y., Sanford, W.E., Heilig, A., Stagnitti, F., and Walter, M.F. 1999; Bussière, Aubertin, Chapuis. 2003*). The
37 water movement restriction across the interface of these layers occurs due to the contrast in unsaturated hydraulic
38 properties employed by the materials (*Tang, J., Taro, U., Huang, D., Xie, J., and Tao, S. 2020, Li. N., Jiang. H., and Li.*
39 *X. 2020*).

40 The present study intends to investigate the water balance of a multi-layer earthen cover. The purposes of current
41 research are to minimize leachate transport by infiltrating water and reduce erosion of earthen covers by water and
42 wind. The unsaturated hydraulic performance of the earthen barrier is numerically evaluated under different
43 climatological conditions spanning the past 20 years (2000-2019) in Canada (Windsor)(Fig.1).

44 For this purpose, the useful finite element code HYDRUS-2D was used to investigate the water flux that leaves the
45 barrier. The generated water flux was investigated as vertical infiltration and as lateral flux. The numerical simulation
46 was done for a multi-layer earthen barrier. Design parameters, such as layer thickness and geoenvironmental
47 parameters of materials, follow the "Landfill Gas Collection and Control Regulation" of Ontario.

48 The program used for this study – HYDRUS – is a modeling environment for the analysis of water flow and solute
49 transport in variably saturated porous media. HYDRUS uses computational finite element models for the two- and
50 three-dimensional simulation of solutes and water through said media. The model is supported by an interactive
51 graphics-based interface for data-preprocessing, generation of structured and unstructured finite element mesh,
52 and graphic presentation of the results (*Šimůnek, J., van Genuchten, M. Th. and Šejna, M. 2012*).

53 **2. Materials and Methods**

54 **2.1. Barrier Design**

55 Earthen barriers are usually made up of fine-grained sediment overlying coarse-textured soil. The simulated multi-
56 layer capillary barrier consists of natural materials. The selected materials for this study's modelled barrier are clay
57 loam as the seepage control layer, sand as the moisture retention layer, and gravel as the capillary break layer.
58 Additionally, the layer has a slope of 10%, which, based on "Landfill Gas Collection and Control Regulation" of
59 Ontario, the slope can be between 5% and 25%. The slope performance includes water percolation discharge and
60 lateral diversion. The purpose of the top 0.6 m of clay loam is to serve as the seepage control layer to reduce water
61 percolation, bio-intrusion, and water storage, as well as promote plant growth. The underlying layers include 0.4 m
62 of sand and 0.2 m of gravel that are used as capillary break, to prevent downward infiltration of water as well as
63 excess-water discharge. A cross-section of the designed cover is depicted in Fig.2.

64 An essential part of protective earthen cover is vegetation. In this study, evapotranspiration was indirectly
65 accounted for by using the Hargreaves equation (*Jensen, D. T., G. H. Hargreaves, B. Temesgen, R. G. Allen. 1997;*
66 *Šimůnek 2015*). Likewise, soil evaporation and plant transpiration were calculated using Beer's law, which divides
67 the solar radiation component of the energy budget via interception by the canopy (*Ritchie, 1972, Asadi, Ali,*
68 *Vivek K. Arora, Joe R. Melton, and Paul Bartlett. 2018*).

69
70 The numerical analysis of water flow was confined to the three-layered barrier. The numerical simulation was done
71 by a fine computational mesh, as demonstrated in the different layers. This is an essential part in the transient state

72 of water flow modelling. Also, it is to be noted that the hydraulic properties of unsaturated materials have a non-
73 linear behavior.

74 Knowledge about the hydraulic properties of the chosen barrier materials – clay loam, sand, and gravel – help to
75 understand the hydraulic behavior of the layers. The intended hydraulic properties are soil water retention curve,
76 $\theta(h)$; and hydraulic conductivity function, $K(h)$; where h is pressure head, θ is volumetric water content, and K is
77 hydraulic conductivity. The hydraulic properties of the materials were not obtained based on real measurements.
78 The hydraulic properties of clay loam were obtained by RETC code (*van Genuchten, M.Th., Leij, F.J., and Yates, S.R.*
79 *1991*), while the hydraulic properties of sand and gravel were selected from literature. A short review of the selected
80 hydraulic properties is presented below (parameter values will be discussed in Table 1).

81 2.2. Governing Flow Equation

82 Based on the two-dimensional isothermal uniform Darcian flow in a porous medium with variably saturated
83 conditions, which the air phase does not consider in the water flow process, Richards' equation has been modified
84 to introduce the governing flow equation. The modified Richard's equation, then, appears as:

$$85 \quad \frac{\partial \theta}{\partial t} = \frac{\partial}{\partial x_i} \left[K \left(K_{ij}^A \frac{\partial h}{\partial x_j} + K_{iz}^A \right) \right] - S \quad (1)$$

86 where θ is the volumetric water content $\left[\frac{L^3}{L^{-3}} \right]$, h is the pressure head [L], S is a sink term for plant water uptake
87 $[T^{-1}]$, x_i ($i=1,2$) are the spatial coordinates [L], t is time [T], K_{ij}^A is anisotropy tensor to account for the anisotropy
88 medium K^A , and K is the unsaturated hydraulic conductivity function $[LT^{-1}]$. The unsaturated hydraulic
89 conductivity function is presented by

$$90 \quad K(h, x, z) = K_s(x, z) K_r(h, x, z) \quad (2)$$

91 where K_r is the relative hydraulic conductivity and K_s the saturated hydraulic conductivity $[LT^{-1}]$. Applying equation
92 (3) to planar flow in a vertical cross-section would then introduce $x_1 = x$ as the horizontal coordinate and $x_2 = z$
93 as the vertical coordinate, the latter coordinate taken to be positive upward. (*Šimůnek, J., van Genuchten, M. Th.*
94 *and Šejna, M. 2012*).

95 **2.3. Unsaturated soil hydraulic properties**

96 The RETC Code is a computer program to analyze or predict the unsaturated hydraulic properties of soils: Water
 97 Retention Curve, $\theta(h)$; and Hydraulic Conductivity Function, $K(h)$. The hydraulic properties of soils are the key
 98 parameters used in water flow quantity analysis in unsaturated soils (*van Genuchten, M.Th., Leij, F.J., and Yates, S.R.*
 99 *1991*). The soil-hydraulic functions used by van-Genuchten [1980] included the statistical pore-size distribution
 100 model of Mualem [1976] to obtain a predictive equation for the unsaturated hydraulic conductivity function in terms
 101 of soil water retention parameters. The expressions of van-Genuchten [1980] are presented by equations (3), (4),
 102 and (5).

$$\theta_h = \begin{cases} \theta_r + \frac{\theta_s - \theta_r}{[1 + |\alpha h|^n]^m} & h < 0 \\ \theta_s & h \geq 0 \end{cases} \quad (3)$$

$$K(h) = K_s S_e^l [1 - (1 - S_e^{1/m})^m]^2 \quad (4)$$

$$\text{Where } m=1-1/n \quad (5)$$

103 The above equations contain six independent parameters:

104 θ_r (residual water content), θ_s (saturated water content), α , n (constant that define the curve shape),

105 K_s (saturated hydraulic conductivity), and l (pore-connectivity parameter). The pore-connectivity parameter in the
 106 hydraulic conductivity function was estimated [Mualem, 1976] to be about 0.5 as an average for many soils.

107 As depicted in Fig.4, there are vast differences among the shape of soil hydraulic functions and the hydraulic behavior
 108 of soils.

109 The trail of soil types is as follows (Fig.2): clay loam (upper material), sand (intermediate material) and gravel (bottom
 110 material). The barrier is characterized by a slope of 10%, a width of 10 m, and a depth of 1.2 m that includes the
 111 three mentioned layers of various thickness. The barrier consists of 4350 triangular elements present in areas where
 112 the highest fluxes occurred and where the more minute elements were considered.

113 **2.4. Initial and boundary conditions**

114 The solution of the modified- Richards' equation used in this research requires knowledge of the initial water
 115 content in the flow domain. The following equation serves that purpose.

$$116 \quad \theta(x, z, t) = \theta_0(x, z) \text{ for } t = 0 \quad (6)$$

117 In (6), θ_0 is a determined function of x and z . There are three types of conditions that are described by HYDRUS to
 118 evaluate the system-independent interactions along the boundaries of the flow region. The pressure head
 119 (Dirichlet type) boundary conditions can be presented as follows:

$$120 \quad h(x, z, t) = \psi(x, z, t) \text{ for } (x, Z) \in \Gamma_D \quad (7)$$

121 The described flux (Neumann type) boundary condition is presented by

$$122 \quad -K \left[K_{ij}^A \frac{\partial h}{\partial x_j} + K_{iz}^A \right] n_i = \sigma_1(x, z, t) \text{ for } (x, Z) \in \Gamma_N \quad (8)$$

123 As well as the described gradient boundary conditions are presented by

$$124 \quad \left[K_{ij}^A \frac{\partial h}{\partial x_j} + K_{iz}^A \right] n_i = \sigma_2(x, z, t) \text{ for } (x, Z) \in \Gamma_g \quad (9)$$

125 The Dirichlet, Neumann, and gradient type boundary segments are defined by $\Gamma_D, \Gamma_N, \Gamma_g$ respectively; ψ [L], σ_1 [LT-
 126 1], and σ_2 [-] are prescribed functions of x, z and t ; and n_i are the segments of the outward unit vector normal to
 127 boundary Γ_N or Γ_g (Šimůnek, J., van Genuchten, M. Th. and Šejna, M. 2012). In the HYDRUS program, the simulation
 128 of free drainage from a deep soil profile can be presented by the implementation of a gradient boundary condition
 129 in terms of a unit vertical hydraulic gradient. This circumstance is usually presented in the vadose zone studies (Sisson
 130 1987; McCord 1991; Šimůnek, J., van Genuchten, M. Th. and Šejna, M. 2012).

131 In the present numerical simulation, the atmospheric boundary conditions are assigned to the top boundary and the
 132 free drainage boundary conditions are assigned to the bottom boundary (Fig.2). In the atmospheric boundary
 133 conditions, the external conditions control the potential fluid flux that moves across the intended boundary. Also,
 134 the actual flux depends on the dominant soil moisture conditions. The numerical solution of the modified form of
 135 Richards' equation is as follows:

136
$$\left| K \left[K_{ij}^A \frac{\partial h}{\partial x_j} + K_{iz}^A \right] n_i \right| \leq E \quad (10)$$

137
$$h_A \leq h \leq h_S \quad (11)$$

138 where E is the maximum potential rate of infiltration or evaporation under the current atmospheric conditions, h is
 139 the pressure head at the soil surface, and h_A and h_S are the minimum and maximum pressure heads allowed under
 140 the dominant soil conditions — respectively. Based on the HYDRUS assumption, any excess water on the soil surface
 141 is immediately eliminated. (Neuman, S. P., R. A. Feddes, and E. Bresler. 1974; Šimůnek, J., van Genuchten, M. Th. and
 142 Šejna, M. 2012). Gradient type boundary conditions, exclusively as the unit gradient boundary condition or the Free
 143 Drainage boundary condition, were implemented by HYDRUS. Whenever the flow is contrary to the particular axis,
 144 the gradients in the x-direction (from right to left) and in the y-direction (from back to front) are positive (Šimůnek,
 145 J., van Genuchten, M. Th. and Šejna, M. 2012). The long-term daily climatological data – comprised of precipitation,
 146 evaporation, and transpiration — is assigned to the top boundary condition (the meteorological stations are
 147 "Windsor Riverside" and "Windsor A" which are situated in Windsor city, Ontario province, Canada), while a unit
 148 vertical gradient corresponds to simulate free drainage in the bottom boundary condition. The right and left
 149 boundaries of the domain assume zero flux boundary conditions. The initial water content for each soil type is
 150 included in Table 1 and it was considered throughout the barrier.

151 **2.5. Numerical solution strategy**

152 The Galerkin finite element method with linear basis functions was used to obtain the solution for the modified form
 153 of Richards' equation dependent on the imposed initial water content and boundary conditions. Either the Gaussian
 154 elimination or the conjugate gradient method was used to solve each iteration system of linearized algebraic
 155 equations. The iterative process was continued until a satisfactory degree of convergence was obtained; i.e. until at
 156 all nodes in the unsaturated region, the absolute value of change in water content between two consecutive
 157 iterations became less than some small value determined by the imposed absolute value of water content
 158 $(0.0003 \frac{cm^3}{cm^3})$ tolerance.

159 **2.6. Water balance computations**

160 Water balance computations were performed 480 times for the three subregions of flow domain. The water balance
 161 information for each subregion is comprised of: the actual volume of water, $V(cm^2)$, in the respective subregion;
 162 and the rate, $O(cm^2/day)$, of inflow or outflow to or from the subregion. V and O are given by

163
$$V = \sum_e \kappa \frac{\theta_i + \theta_j + \theta_k}{3} \text{ for 2D (12)}$$

164
$$O = \frac{V_{new} - V_{old}}{\Delta t} \text{ (13)}$$

165 where $\theta_i, \theta_j, \theta_k$ are calculated water contents at the corner nodes of element e , and where V_{new} and V_{old} are
 166 volumes of water in the subregion computed at the current and previous time levels, respectively. The absolute
 167 error in the mass balance is computed by

168
$$\varepsilon_a^w = V_t - V_0 + S_t \int_0^t T_a dt - \int_0^t \sum_{n_r} Q_n dt \text{ (14)}$$

169 where V_t and V_0 are the volumes of water in the flow domain at time t and zero, respectively, as calculated with
 170 equation (12). The third term on the right side of the equation represents the cumulative root water uptake amount,
 171 while the fourth term gives the cumulative flux through nodes (n_r) located along the boundary of the flow domain
 172 or at internal source and sink nodes.

173 The accuracy of the numerical solution is evaluated in terms of the relative error, ε_r^w [%], in the water mass balance
 174 as follows:

175
$$\varepsilon_r^w = \frac{|\varepsilon_a^w|}{\max[\sum_e |V_0^e - V_t^e|, S_t \int_0^t T_a dt - \int_0^t \sum_{n_r} |Q_n| dt]} \text{ (15)}$$

176 where V_t^e and V_0^e are the volumes of water in element e at times t and zero, respectively. Note that HYDRUS does
 177 not relate the absolute error to the volume of water in the flow domain, but instead to the maximum value of two
 178 quantities. The first quantity represents the sum of the absolute changes in water content over all elements, whereas
 179 the second quantity is the sum of the absolute values of all fluxes in and out of the flow domain. This criterion is
 180 much stricter than the usual criterion involving the total volume of water in the flow domain; this is because

181 cumulative boundary fluxes are often much smaller than the volume in the domain, especially at the beginning of
182 the simulation.

183 Also, the water balance was calculated throughout the flow domain, made up of the three subregions previously
184 adopted.

185 **3. Results and discussion**

186 Based on assigned initial water content and boundary conditions, flow in the multi-layer earthen cover was transient.
187 The mean pressure head in all layers is not constant (Fig.5). The water balance error at transient state, computed
188 with equation (15), reveals the water balance error to be variable between 0.028% and 0.156%.

189 The total flux that leaves the simulation domain across the bottom boundary presents several noticeable features
190 (Fig. 5). The main reasons that explain water drainage are water infiltration into the barrier, run-off from the sloping
191 soil, and a rapid decrease in flux due to water drainage from the bottom. When the flux increased and was followed
192 by a decrease, water drainage from either sand or gravel layers was considered.

193 The spatial variation of the Darcy flux across the bottom boundary is displayed in Fig. 6. A decreasing behavior was
194 observed in an area close to the left and right boundary of the barrier. This is the result of contrasting hydraulic
195 properties below the lower end of the sand layer. Conclusively, a lateral hydraulic gradient exists between the clay
196 loam and sand, creating a lateral flux into the sand (Fig. 7). Based on the average flux across the bottom boundary
197 (free drainage boundary condition) the highest mean velocity occurs in week 867 from 1043 weeks. Hence, the
198 highest velocity in the respective time occurs at the bottom of the 3rd layer (it occurs 860 cm from the left boundary
199 of the simulation). The lower peaks in the bottom layer are observed approximately 20 cm from the left boundary
200 and 20 cm from the right boundary in the gravel layer (Fig.8).

201 Lastly, the cumulative flux across the bottom boundary was calculated. The total cumulative flux equals the
202 summation of the fluxes of each element, times the element length (L^2T^{-1}). This was equal to $1505.5 \text{ cm}^2/\text{day}$.
203 This value equals 78.91% of the cumulative net rainfall that entered the barrier from the atmospheric boundary.
204 Therefore, 21.09% of the rainfall can be considered runoff (Fig.9).

205 The simulated mean pressure head for all barrier layers at transient state was summarized in table 2.

206 As expected, the second layer (moisture retention layer) held more water, and the mean pressure head in the third
 207 layer held less, due to the high retention capacity of the sand layer and the lateral diversion phenomenon.

208 Based on Darcy fluid velocities (Fig.7), fluxes in the sand layer are parallel to the slope. In the intended times, the
 209 significant amount of water that passed through the sand layer was laterally diverted. The capillary barrier effect
 210 was depicted at $t=2008$ days and $t=6023$ days when a considerable volume of water was diverted along the interface
 211 of the moisture retention layer and the capillary break layer. The capillary barrier effect was presented in the
 212 interface when the fine-grained material overlaid the coarse-grained one. In unsaturated conditions, the pressure
 213 head in the fine-grained layer was higher than the pressure head in the coarse-grained material. As a result, the
 214 moisture retention layer could store water. Furthermore, water was diverted laterally due to the slope of the layer.

215 Based on the mean pressure head for various climatological conditions, the seepage control layer was -326.91 cm at
 216 its lowest and -11.75 cm at its highest (Fig.10). Based on the water retention curve shape of the clay loam (Fig.3),
 217 the negative pressure heads have a noticeable effect on water content and degree of saturation.

218 The profile of water content (Fig.11) along a perpendicular line at 250 cm from the left boundary of the earthen
 219 cover was depicted for changeable climatological conditions. The initial water content was calculated from
 220 $\theta_i = ((\theta_s - \theta_r) + \theta_r)(n^{-0.6(2+\log K_s)})$ where θ_i , θ_r , θ_s , K_s , n are initial water content, residual water content,
 221 saturated water content, saturated hydraulic conductivity and a constant that define the shape of the curve,
 222 respectively. In the first layer, the infiltration developed between $t=1825$ days and $t=7300$ days. The water content
 223 in the top 22.7 cm of the sand layer showed a steady-state behavior, but then reduced suddenly. This event is
 224 introduced as the main reason for the lateral diversion of water. The water content in the gravel layer was reduced
 225 as well, but its behavior was not linear, and the bottom of the layer was not saturated.

226 In this calculation, the distribution of hydraulic properties was assumed to be homogeneous .

227 4. Conclusions

228 Based on the numerical analysis results at transient state conditions, the lateral drainage of water occurred at the
 229 interface between the sand layer and the gravel layer. In the current transient state for variable climatological

230 conditions, 21% of water infiltration was converted to lateral drainage. Also, the mean flux that permeated the
231 bottom boundary was 206.70 cm/day (2.39×10^{-6} m/s). Hence, this mean flux had minimal effect in the variable
232 climatological conditions. The performance of this protective earthen cover can, then, be guaranteed due to the
233 current climatological conditions.

234 The results of negative pressure head in the seepage control layer showed that this layer is usually under unsaturated
235 conditions. Hence, this circumstance will cause the formation of cracks in the clay.

236 Future studies should address the investigation of multi-layered earthen covers using experimental data from
237 laboratory prototypes or field-scale studies. In such studies, numerical calculations – such as the ones presented
238 here – may be appropriate in selecting improved barrier designs.

239 **5. Data Availability Statement**

240 Some or all data, models, and code that support the findings of this study are available through the corresponding
241 author upon reasonable request.

242 **6. Author contributions**

243 All authors contributed to the study conception and design. Material preparation, data collection and analysis were
244 performed by Mohammad Ali Hagh Shenaa, Hassan Sharafi. The first draft of the manuscript was written by
245 Mohammad Ali Hagh Shenaa and Ana Colindres. All authors commented on previous versions of the manuscript. All
246 authors read and approved the final manuscript.

247 **7. Acknowledgments**

248 This research has been made possible entirely through personal funding.

249 **8. References**

250 Aubertin, M. Cifuentes, E. Apithy, S.A. Bussière, B. Molson, J. Chapuis, R.P. 2009. "Analyses of Water Diversion along
251 Inclined Covers with Capillary Barrier Effects." Canadian Geotechnical Journal 46(10): 1146–64.

- 252 Asaadi, Ali, Vivek K. Arora, Joe R. Melton, and Paul Bartlett. 2018. "An Improved Parameterization of Leaf Area Index
253 (LAI) Seasonality in the Canadian Land Surface Scheme (CLASS) and Canadian Terrestrial Ecosystem Model (CTEM)
254 Modelling Framework." *Biogeosciences* 15 (22): 6885–6907. <https://doi.org/10.5194/bg-15-6885-2018>.
- 255 Bussie`re, B., Aubertin, M., and Chapuis, R.P. 2003. The behavior of inclined covers used as oxygen barriers. *Canadian
256 Geotechnical Journal*, 40(3): 512–535. doi:10.1139/t03-001.
- 257 Jensen, D. T., G. H. Hargreaves, B. Temesgen, R. G. Allen. 1997. Computation of Eto under nonideal conditions. - *J. of
258 Irrig. Drainage*, 123, 5, 394-400.
- 259 Khire, M.V., Benson, C.H., and Bosscher, P.J. 2000. Capillary barriers: design variables and water balance. *Journal of
260 Geotechnical and Geoenvironmental Engineering*, 126(8): 695–708. doi:10.1061/(ASCE)1090-
261 0241(2000)126:8(695).
- 262 Li. N., Jiang. H., and Li. X. 2020. Behaviour of Capillary Barrier Covers Subjected to Rainfall with Different Patterns.
263 *Water Journal*.
- 264 Selim, H.M. 1988. Water flow in layered soils with sloping surface. *Journal of Irrigation and Drainage Engineering*,
265 114: 442–462.
- 266 Mallants, D. Volckaert, G. Marivoet, J. 1999. "Sensitivity of protective barrier performance to changes in rainfall
267 rate." *Waste Management* 19: 467-475.
- 268 Morris, C.E., and Stormont, J.C. 1997. Capillary barriers and Subtitle D covers: estimating equivalency. *Journal of
269 Environmental Engineering*, 123(1): 3–10. doi:10.1061/(ASCE)0733-9372(1997) 123:1(3).
- 270 Mualem, Y. 1976. "A New Model for Predicting the Hydraulic Conductivity of Unsaturated Porous Media." *Water
271 Resources Research* 12: 513–22.
- 272 Nieber, J.L., and Walter, M.F. 1981. Two-dimensional soil moisture flow in a sloping rectangular region: experimental
273 and numerical studies. *Water Resources Research*, 17: 1722–1730.

- 274 Neuman, S. P., R. A. Feddes, and E. Bresler, Finite element simulation of flow in saturated-unsaturated soils
275 considering water uptake by plants, Third Annual Report, Project No. A10-SWC-77, Hydraulic Engineering Lab.,
276 Technion, Haifa, Israel, 1974.
- 277 Ritchie, J. T. 1972. Model for predicting evaporation from a row crop with incomplete cover. - Water Resour. Res.,
278 8, 5, 1204-1213.
- 279 Šimůnek, J., van Genuchten, M. Th. and Šejna, M. 2012. The HYDRUS Software Package for Simulating the Two- and
280 Three-Dimensional Movement of Water, Heat, and Multiple Solutes in Variably Saturated Porous Media (Technical
281 Manual Version 2.0)
- 283 Šimůnek, J. 2015. Estimating groundwater recharge using HYDRUS-1D. In: Engineering geology and Hydrogeology,
284 Sofia, pp 25–36
- 285 Stagnitti, F., Parlange, J.-Y., Steenhuis, T.S., Parlange, M.B., and Rose, C.W. 1992. A mathematical model of hillslope
286 and watershed discharge. Water Resources Research, 28: 2111–2122.
- 287 Steenhuis, T.S., Parlange, J.-Y., Sanford, W.E., Heilig, A., Stagnitti, F., and Walter, M.F. 1999. Can we distinguish
288 Richards' and Boussinesq's equations for hillslopes: The coweeta experiment revisited. Water Resources Research,
289 35: 589–593.
- 290 *Tang, J., Taro, U., Huang, D., Xie, J., and Tao, S. 2020. Physical Model Experiments on Water Infiltration and*
291 *Failure Modes in Multi-Layered Slopes under Heavy Rainfall. Applied Science Journal.*
- 292 van Genuchten, M. Th. 1980. "A Closed-Form Equation for Predicting the Hydraulic Conductivity of Unsaturated
293 Soils." Soil Science Society of America Journal. <https://doi.org/10.2136/sssaj1980.03615995004400050002x>.
- 294 van Genuchten, M.Th., Leij, F.J., and Yates, S.R. 1991. "The RETC Code for Quantifying the Hydraulic Functions of
295 Unsaturated Soils." Vol. EPA/600/2-. U.S. Department of Agriculture, Agriculture Research Service.
- 296 Zaradny, H. 1993. Groundwater flow in saturated and unsaturated soil. Edited by R.B. Zeidler. Balkema, Rotterdam,
297 the Netherlands.

- 298 Zaslavsky, D., and Sinai, G. 1981a. Surface hydrology: III — Causes of lateral flow. *Journal of the Hydraulics Division*,
299 ASCE, 107(HY1): 37–52.
- 300 Zaslavsky, D., and Sinai, G. 1981b. Surface hydrology: IV — Flow in sloping, layered soil. *Journal of the Hydraulics*
301 *Division*, ASCE, 107(HY1): 53–64.

Table 1

Soil water retention and hydraulic conductivity parameters and initial soil water content (θ_i) for soil types used in the water flow calculations

| Parameter | Perth Clay Loam | Clinton Sand | Clinton Gravel |
|-----------------------|--|--------------------|--------------------|
| Material number | 1 | 2 | 3 |
| Layer number | 1 | 2 | 3 |
| Layer thickness(cm) | 60 | 40 | 20 |
| $\theta_r(cm^3/cm^3)$ | 0.0696 | 0 | 0.0016 |
| $\theta_s(cm^3/cm^3)$ | 0.4142 | 0.2323 | 0.2378 |
| $\alpha (cm)^{-1}$ | 0.0115 | 1.1956 | 0.3580 |
| n | 1.4562 | 2.4925 | 2.1014 |
| $K_s (\frac{cm}{d})$ | 7.37 | 3196.8 | 43200 |
| Source | <i>van Genuchten, M.Th., Leij, F.J., and Yates, S.R. 1991., Richards and Morwick 1949</i> | <i>Parent 2003</i> | <i>Parent 2003</i> |
| $\theta_i(cm^3/cm^3)$ | 0.2501 | 0.01138 | 0.01389 |
| Source | <i>Twarakavi, N. K. C, M. Sakai, and J. Šimůnek. 2009; Šimůnek, J., van Genuchten, M. Th. and Šejna, M. 2012</i> | | |

Table 2

Summary of simulation results: hmean is mean pressure head,

| | | Layers | | |
|------|----------|--------|--------|---------|
| | | 1 | 2 | 3 |
| Time | Property | | | |
| 183 | hMean | -36.35 | -10.84 | -59.80 |
| 913 | | -61.11 | -27.03 | -146.49 |
| 1278 | | -39.77 | -19.81 | -107.93 |
| 1643 | | -51.59 | -20.19 | -103.68 |
| 2008 | | -73.07 | -34.07 | -176.60 |
| 2373 | | -51.40 | -19.37 | -92.72 |
| 2738 | | -39.16 | -12.67 | -57.83 |
| 3833 | | -40.17 | -12.89 | -59.38 |
| 4563 | | -54.22 | -19.00 | -88.89 |
| 6023 | | -93.04 | -39.18 | -192.37 |
| 6753 | | -41.84 | -13.79 | -63.14 |



Fig 1. The map of Windsor

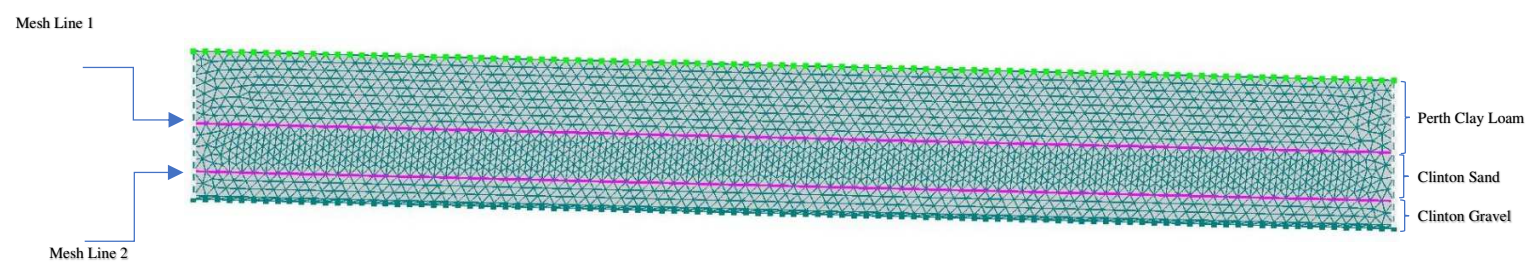


Fig 2. Distribution of soil layers within the barrier (from top to bottom): Perth Clay Loam (60 cm); Clinton Sand (40 cm); Clinton Gravel (20 cm)

An essential part of protective earthen cover is vegetation. In this present study evapotranspiration was indirectly

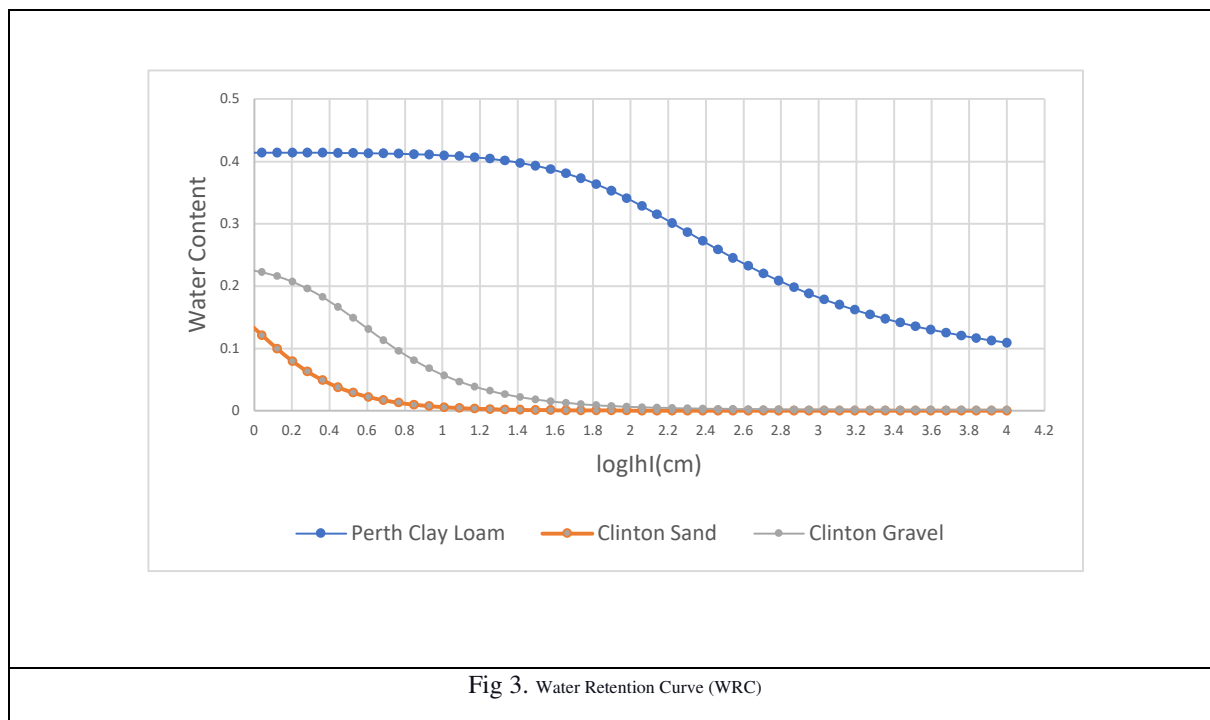
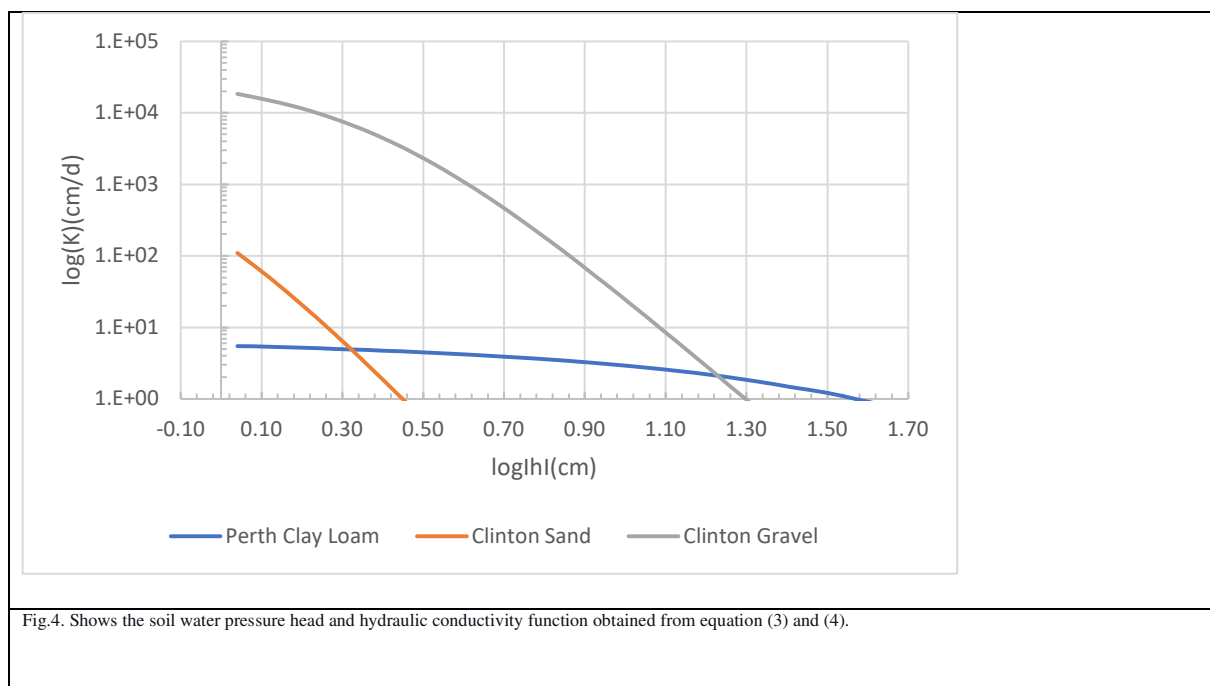
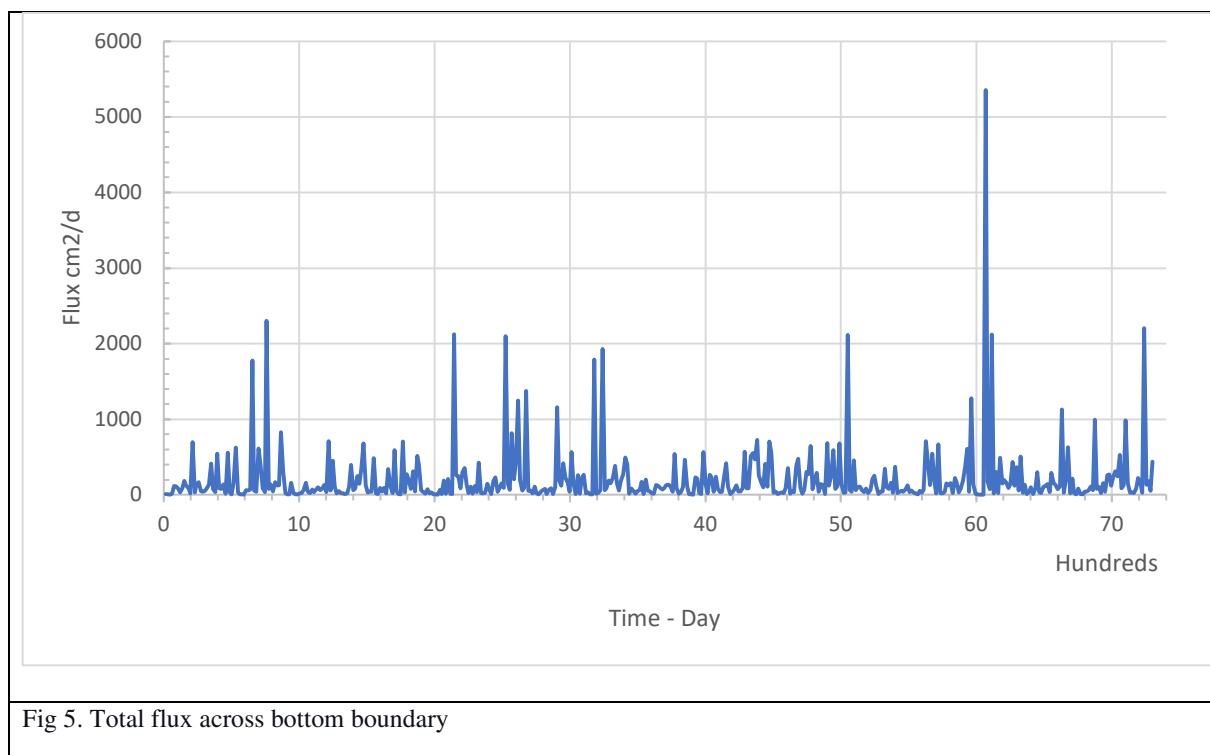


Fig 3. Water Retention Curve (WRC)





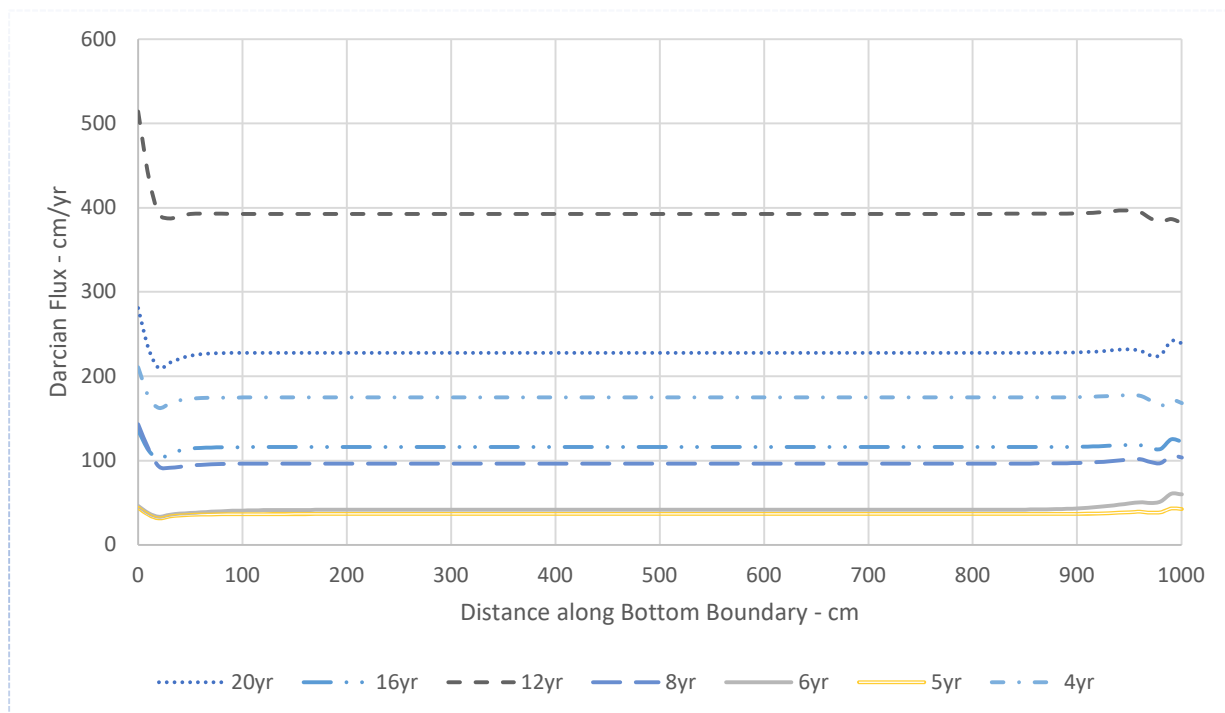


Fig 6. Variation of the Darcian flux along the bottom boundary

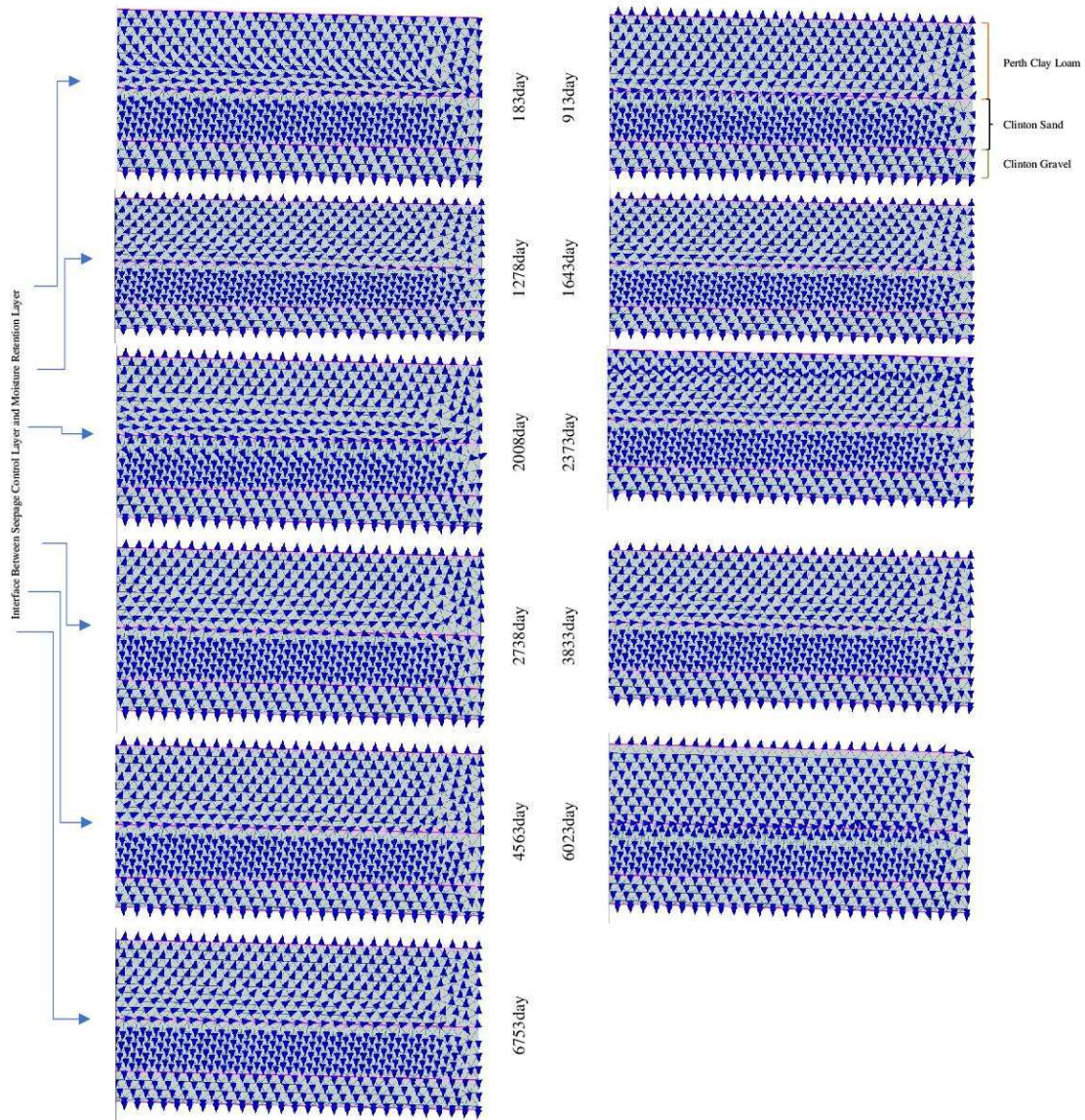
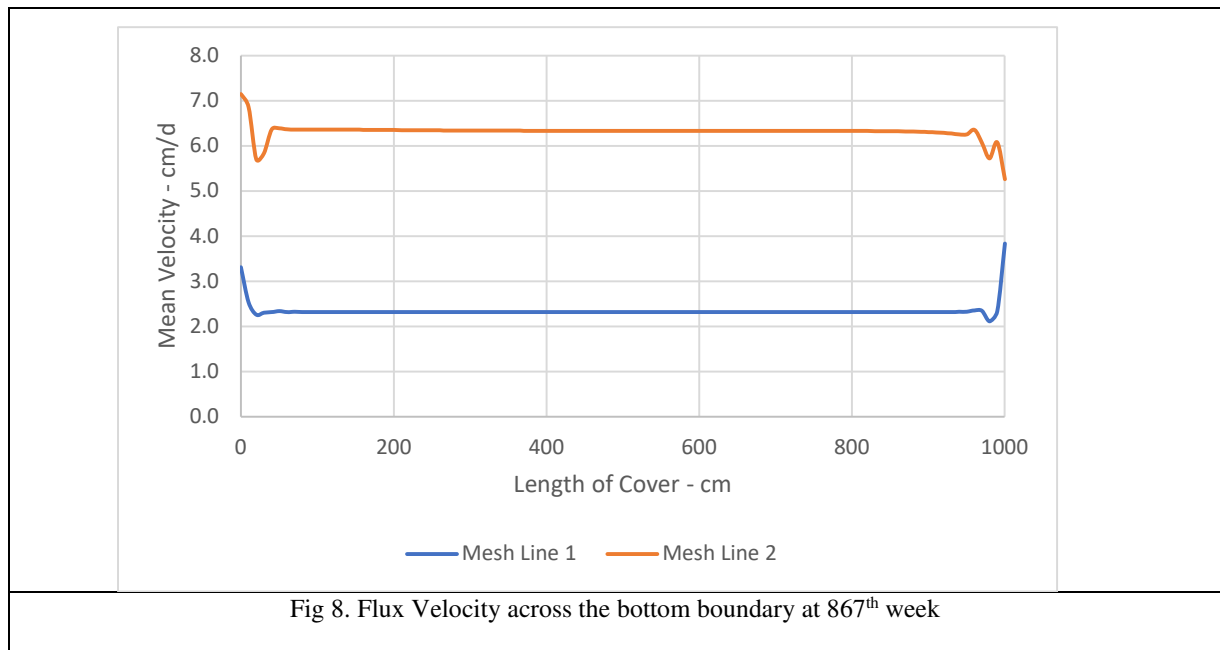


Fig 7. Darcian velocity at eleven different times for various climatological conditions.
(Lateral Drainage depicted in the interface between seepage control layer and moisture retention layer)



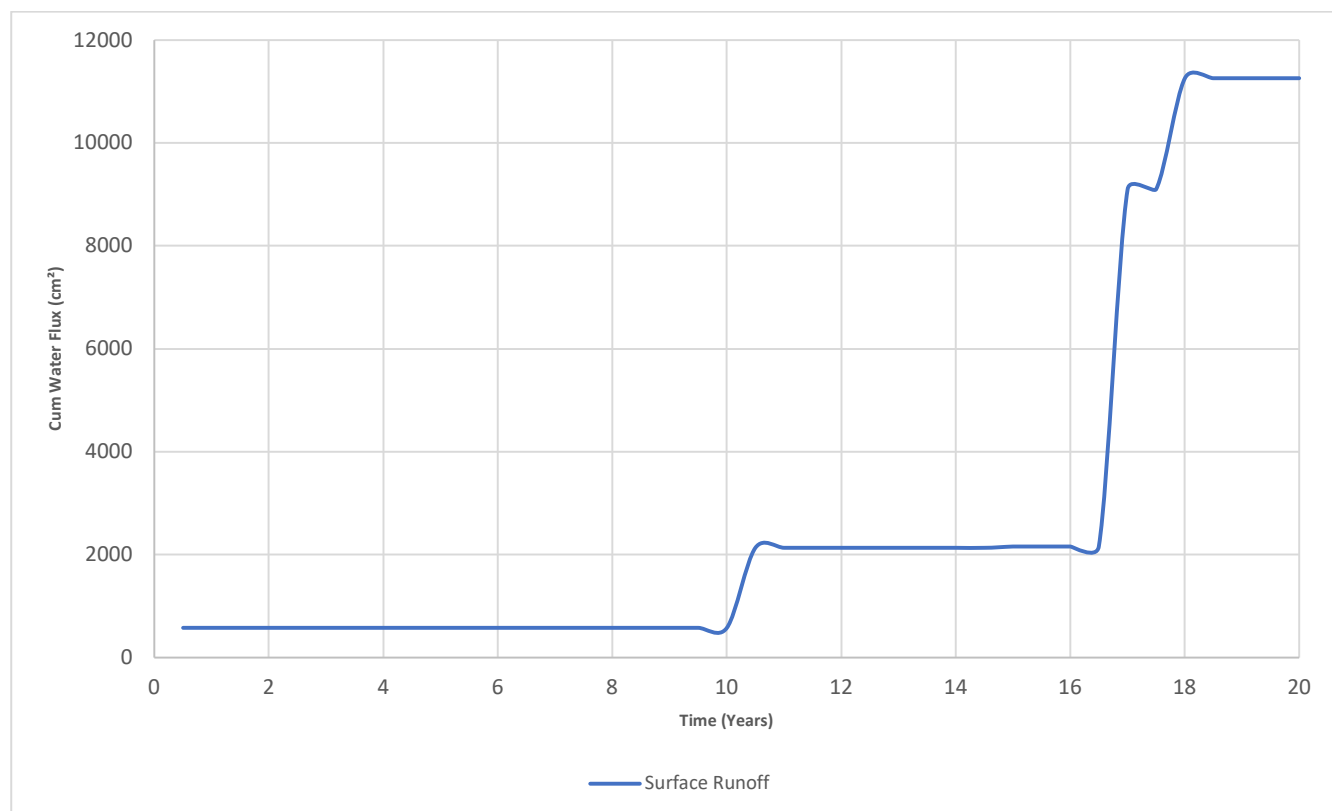


Fig 9. Cumulative Surface Runoff

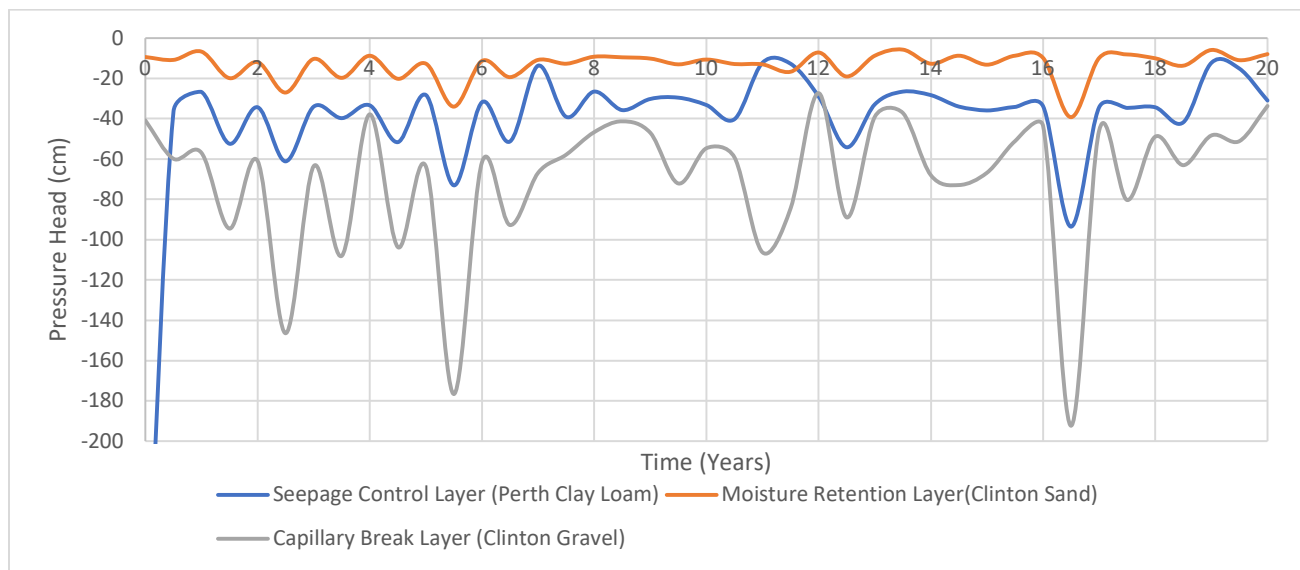


Fig. 10. Mean pressure head in layers

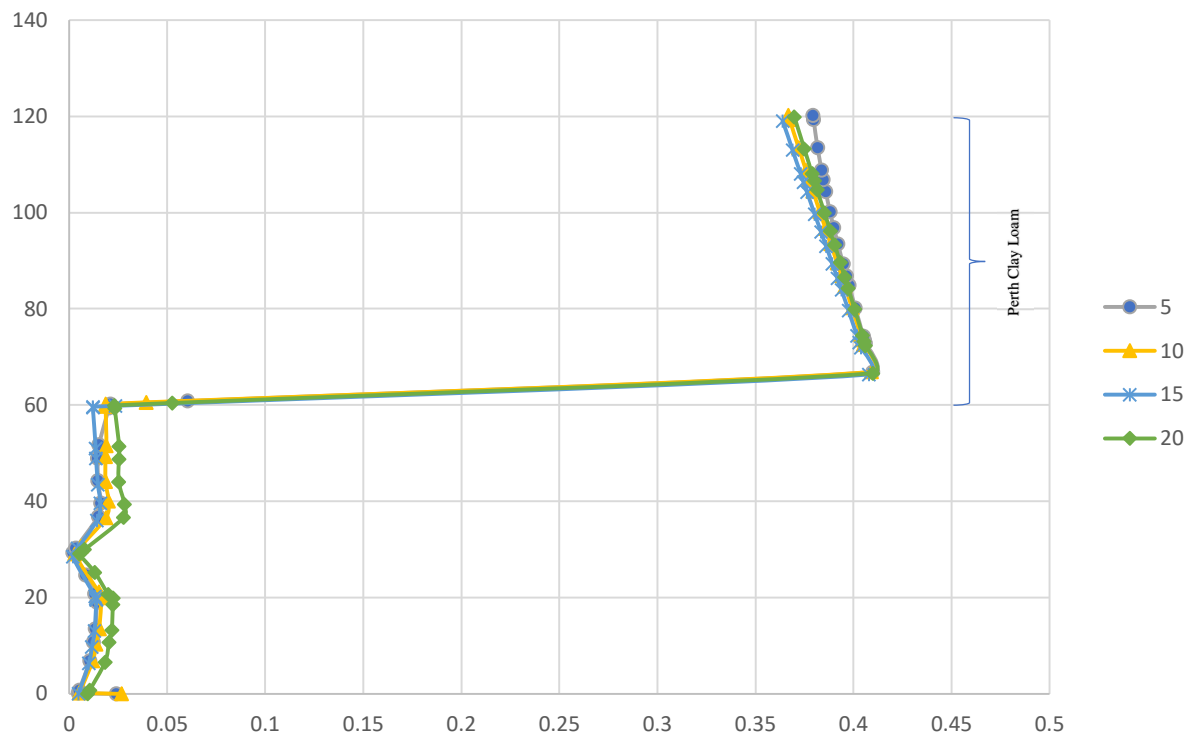


Fig 11. Soil water content versus depth at four different times along a vertical line at $x=250$ cm from the left boundary